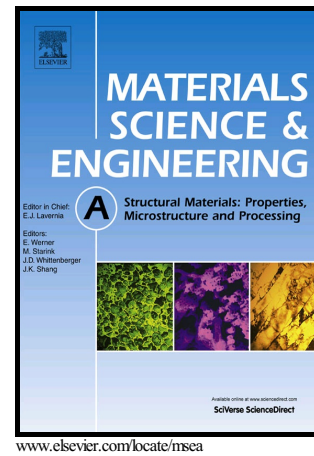


Author's Accepted Manuscript

Laser powder bed fusion of Hastelloy X: effects of hot isostatic pressing and the hot cracking mechanism

Quanquan Han, Raya Mertens, Maria L. Montero-Sistiaga, Shoufeng Yang, Rossitza Setchi, Kim Vanmeensel, Brecht Van Hooreweder, Sam L. Evans, Haiyang Fan



PII: S0921-5093(18)30924-9
DOI: <https://doi.org/10.1016/j.msea.2018.07.008>
Reference: MSA36672

To appear in: *Materials Science & Engineering A*

Received date: 21 May 2018
Revised date: 2 July 2018
Accepted date: 3 July 2018

Cite this article as: Quanquan Han, Raya Mertens, Maria L. Montero-Sistiaga, Shoufeng Yang, Rossitza Setchi, Kim Vanmeensel, Brecht Van Hooreweder, Sam L. Evans and Haiyang Fan, Laser powder bed fusion of Hastelloy X: effects of hot isostatic pressing and the hot cracking mechanism, *Materials Science & Engineering A*, <https://doi.org/10.1016/j.msea.2018.07.008>

This is a PDF file of an unedited manuscript that has been accepted for publication. As a service to our customers we are providing this early version of the manuscript. The manuscript will undergo copyediting, typesetting, and review of the resulting galley proof before it is published in its final citable form. Please note that during the production process errors may be discovered which could affect the content, and all legal disclaimers that apply to the journal pertain.

Laser powder bed fusion of Hastelloy X: effects of hot isostatic pressing and the hot cracking mechanism

Quanquan Han^a, Raya Mertens^b, Maria L. Montero-Sistiaga^{c,d}, Shoufeng Yang^{b*}, Rossitza Setchi^{a*}, Kim Vanmeensel^c, Brecht Van Hooreweder^b, Sam L. Evans^a, Haiyang Fan^b

^aCardiff School of Engineering, Cardiff University, Cardiff CF24 3AA, UK

^bDepartment of Mechanical Engineering and Flanders Make, KU Leuven, Celestijnenlaan 300B, box 2420, Heverlee B-3001, Leuven, Belgium

^cDepartment of Materials Engineering, KU Leuven, Kasteelpark Arenberg 44, box 2450, Heverlee B-3001, Belgium

^dENGIE Laborelec, Rodestraat 125, Linkebeek B1630, Belgium

Corresponding authors: Rossitza Setchi: Setchi@cardiff.ac.uk, +44(0)2920875720

Shoufeng Yang: Shoufeng.yang@kuleuven.be, +3216324999

Abstract

Hastelloy X is the trademark for a nickel-based, high-temperature superalloy that is increasingly applied in gas turbine engines because of its exceptional combination of oxidation resistance and high-temperature strength. The superalloy suffers from hot cracking susceptibility, however, particularly when processed using additive manufacturing and laser powder bed fusion (LPBF). This paper systematically studies for the first time the effect of post-treatment hot isostatic processing (HIP) on the microstructure and mechanical properties of LPBF-fabricated Hastelloy X, with an emphasis on fatigue performance. The experimental results demonstrate that despite the very small number of remaining gas-filled micropores due to pressure counteraction, the high temperature and high pressure during the HIP process promote recrystallisation and closing of the internal microcracks and gas-free pores. The HIP-processed specimens are shown to be roughly 130 MPa and 60 MPa weaker than the non-processed specimens in yield strength and ultimate tensile strength, respectively. The HIP-processed Hastelloy X exhibits significant improvements in fatigue life, however: the effect of the HIP processing is apparent once the applied stress decreases. This improvement in fatigue performance is attributable to the reduction in stress concentration and residual stress release caused by the HIP process. The paper also studies the hot cracking mechanism and

finds that intergranular microcracks generally occur along high angle grain boundaries; the interdendritic liquid pressure drop between dendrite tip and root is found to be a significant factor in the hot crack mechanism. The significance of this research is in developing a comprehensive understanding of HIP processing on the fatigue behaviour of the LPBF-fabricated Hastelloy X. The insights on the cracking mechanism, which presents a significant step towards using additive manufacturing to produce complex crack-free parts from this superalloy.

Keywords: Laser powder bed fusion, Hastelloy X, Hot isostatic pressing, Fatigue performance, Hot cracking

1. Introduction

Hastelloy X is a solid solution–strengthened, nickel-based superalloy that is widely applied in gas turbine engines because of its exceptional combination of oxidation resistance, formability and high-temperature strength [1,2]. Compared to other nickel-based alloys such as In718 and In625, Hastelloy X is resistant to stress-strain cracking in petrochemical applications and offers good ductility, even at temperatures as high as 1200°C. Because of Hastelloy X's increased hardness and tensile strength, however, fabricating the customised engineering parts used in the aerospace and marine industries is a challenge when using traditional manufacturing techniques [3,4]. Laser powder bed fusion (LPBF) additive manufacturing is an advanced manufacturing technology in which metallic powder is selectively melted layer by layer using a high-power laser [5–8]. The LPBF process offers the ability to fabricate customised Hastelloy X engineering parts.

One problem found in the LPBF of Hastelloy X lies in the material's cracking, however. Some nickel-based superalloys have been found to be particularly susceptible to cracking when processed using LPBF [9–11]. Recent studies have focussed on microcrack minimisation and the hot cracking mechanism in the LPBF of Hastelloy X [12,13]. For instance, Tomus et al. [13] have investigated the effect of minor alloying elements (e.g. Si and Mn) on the crack susceptibility of Hastelloy X. Their study found that an alloy with high Si + Mn content resulted in more microcracks than one with low Si + Mn content. Two primary factors that control crack formation and propagation are generally considered: (i) internal strain

accumulation due to the thermal cycling and (ii) crack formation and propagation during solidification, which is known as 'hot tearing' and is dependent on chemical composition [14].

In another report, however, Marchese et al. [15] pointed out that the Mo-rich carbides that formed at the grain boundaries, together with high thermal residual stress, resulted in hot crack formation along the grain boundaries. Several studies in the literature have discussed possible hot cracking mechanisms. For example, selective electron beam melting has been used to fabricate a non-weldable Ni-based superalloy [16]. That alloy was high in Al and Ti elements, however, which are not present in Hastelloy X. The authors [16] found that hot cracking occurred when two conditions were combined: the presence of (i) a liquid film and (ii) sufficient thermal stress accumulation. The authors also found that hot cracking depended on grain boundary: only high angle grain boundaries, or HAGBs (with misorientation $>15^\circ$), were affected by cracking. Harrison et al. [3], who studied the reduction of microcracks in Hastelloy X by using a fundamental alloy design method, found that the alloy's resistance to cracking could be improved by increasing the concentrations of substitutional solid solution strengthening atoms.

A few studies have investigated the mechanical properties and microstructure of LPBF-fabricated Hastelloy X. For example, Tomus et al. [17] investigated the influence of post-heat treatment on the anisotropy of mechanical behaviour and the microstructure of LPBF-fabricated Hastelloy X. They found that the yield strength drastically decreased (by 200 MPa), while a steady increase (by 10%) of elongation until failure was observed following the heat treatment and/or hot isostatic pressing. Etter et al. [18] studied reductions in mechanical anisotropy through high-temperature heat treatment of LPBF-processed Hastelloy X and observed anisotropy in the Young's modulus, with lower values measured parallel to the build-up direction when different scanning strategies were employed. After heat treatment, the differences between the scanning strategies were nearly eliminated, and the anisotropy of the modulus was greatly reduced.

Tian et al. [19] investigated the influences of process parameters on the surface roughness of Hastelloy X. They found that the large overlap induced by small hatch distances promoted the attachment of particles on the surface, which in turn

increased the surface roughness. For inclined surfaces, the roughness of the up-skin surfaces was virtually unaffected by various scanning powers and speeds in their study, while the roughness of the down-skin surfaces increased with laser power and decreased with scanning speed. Wang [20] studied the tensile and fatigue performances of LPBF-fabricated Hastelloy X using an EOS M270 machine with a relatively high laser power of 200 W. Because only one fatigue sample was used in each level of applied load, however, the fatigue life might not have been representative in that study. The author did not analyse the fatigue-fracture characteristics in detail.

Accordingly, in order to obtain fully dense and crack-free Hastelloy X parts, the present study has systematically examined for the first time the effect of hot isostatic pressing on the microstructure and mechanical properties of LPBF-fabricated Hastelloy X, with an emphasis on fatigue behaviour. In addition, the study examines the hot cracking mechanism and offers insights and practical advice on using LPBF to manufacture crack-free Hastelloy X parts.

2. Materials and procedure

2.1. Materials

The Hastelloy X powder used in this study was obtained from Concept Laser GmbH, with a chemical composition (wt.%) of 23Cr-20Fe-10Mo-2.5Co-1Si-1W-0.05C-bal.Ni. Fig. 1 shows the particle morphology and size of the raw material. The particle size distribution was analysed using a Malvern Mastersizer 3000 (Malvern, UK) with an average measured size of 32 μm .

<Insert Figure 1>

2.2. The powder bed fusion additive manufacturing process

A Concept Laser Mlab machine equipped with a 100 W fibre laser was employed to manufacture the specimens. Materialise Magics software was used for file

preparation. Prior to the fabrication of the tensile and fatigue specimens, a set of cubic samples (10 x 10 x 10 mm³) was manufactured under different conditions in order to determine the optimal scanning speed and hatch spacing. The optimal process parameters that were subsequently used are shown in Table 1. These parameters were employed to manufacture tensile and fatigue specimens for use in the remainder of the study. The specimens were manufactured vertically, which means that the applied loading direction in both tensile and fatigue tests was parallel to the build direction.

<Insert Table 1>

2.3. Material characterisation techniques

The relative density of the as-fabricated cubic samples was measured by the Archimedes method in order to determine the optimal scanning speed and hatch spacing. The four samples with the highest relative densities were then sectioned and polished prior to conducting optical microscopy (OM) and scanning electron microscopy (SEM) observations. For the microstructure analysis, the polished samples were electrochemically etched using oxalic acid for 10 s to reveal molten pool boundaries and solidification microstructures in the secondary electron (SE) SEM mode. The hot cracking phenomenon and distribution were examined in the backscattered electron (BSD) SEM mode. The crystallographic orientation of the samples was investigated using electron backscattered diffraction (EBSD), which was performed on an FEI Nova NanoSEM 450 instrument equipped with a TSL/EDAX system.

Half the fabricated Hastelloy X parts were subjected to hot isostatic pressing (HIP); the HIP processing was carried out at 1155°C for 3 h at 100 MPa argon pressure followed by furnace cooling at Bodycote NV, Sint Niklaas, Belgium. The tensile tests were performed using an Instron 4505 testing machine with a strain rate of 1.5 mm/min at room temperature. The yield strength obtained from the tensile tests was used to determine the stresses that would be employed in the fatigue tests

that followed; five levels of stress (three samples for each level) were used in the fatigue tests. The fatigue tests were conducted using an MTS 858 Mini Bionix II testing machine with a maximum applied load of 20 KN at room temperature. The frequency was set to 10 HZ, and the stress ratio (R) was maintained at 0.1, which was the ratio of minimum stress to maximum stress applied during the fatigue testing. Prior to the fatigue testing, the samples were properly polished, followed by surface roughness measurement using a Talysurf i-Series system.

3. Results

3.1. Relative density

The relative density of the as-fabricated cubic samples as related to scanning speed and hatch spacing are shown in Fig. 2a. When the hatch spacing was maintained at 60 and 75 μm , the relative density measurements increased with the increase in scanning speed until 500 mm/s; the relative density then decreased with further increases in the scanning speed until 800 mm/s. Relatively low scanning speeds (less than 500 mm/s) contributed to lower relative density values under both conditions. This situation could be explained by the keyhole laser working mode that was employed. Fig. 2b shows the molten pools and defects generated by the keyhole laser melting mode at 200 mm/s and 60 μm . Several fairly deep molten pools were observed, which managed to penetrate a few solidified layers. These keyhole-shaped molten pools were found to be associated with the typical keyhole pores. When the hatch spacing was further increased to 90 μm , however, the relative density was found to have decreased from 99.3% to 95.2%, while the scanning speed increased from 200 mm/s to 800 mm/s. The relative density of the HIP-processed sample (90 μm and 200 mm/s) was measured to be as high as 99.98% (also shown in Fig. 2a). The four samples with the highest relative densities (marked in Fig. 2a) were then vertically sectioned to study their defect distributions.

<Insert Figure 2>

The porosity and microcrack distributions of these four samples are shown in Fig. 2c–f. The specimen shown in Fig. 2f had the smallest number of microcracks and pores, which were observed under the different conditions shown in Fig. 2c–f. The cracking appears to have been the primary defect within the LPBF of Hastelloy X. The formation of microcracks is generally accepted to be caused by thermal stress, which is induced by the temperature gradient during the laser irradiation process. The microcracks are generated when the residual stress is greater than the ultimate tensile strength during the rapid solidification process. The cracking mechanism will be discussed in more detail in the next section. A very limited number of residual micropores were observed in the HIP-processed sample; the porosity was calculated to be 0.02% by the ImageJ software (Fig. 2g–h). The OM observations also confirmed that the optimal scanning speed and hatch spacing values in order to fabricate nearly fully dense Hastelloy X were 200 mm/s and 90 μm , respectively. This parameter combination was then employed to fabricate tensile and fatigue specimens for further investigation of their mechanical properties.

3.2. Microstructure

Fig. 3 shows the microstructure of the as-fabricated and HIP-processed Hastelloy X samples, both manufactured using the optimal parameters. Several microcracks and pores were observed in the as-fabricated sample: both columnar dendritic and cellular structures formed because of the difference in solidification rates and laser remelting (Fig. 3a–b). Fairly fine cellular and columnar dendritic structures are expected to favour mechanical performance. In comparison, microcracks were not observed in the HIP-processed sample: the typical columnar dendritic and cellular LPBF microstructures were not present in either the vertical or horizontal sections (Fig. 3c–d).

<Insert Figure 3>

Fig. 4 shows EBSD crystallographic orientation maps and grain size distribution of the as-fabricated and HIP-processed samples, which were useful for further

analysis of HIP processing's effects on the microstructure change. As the EBSD crystallographic orientation map indicates, the grains were oriented almost parallel to the building direction in the as-fabricated sample, which contributed to the formation of epitaxial columnar grains (Fig. 4a). Because of the large number of thermal cycles that were induced by laser remelting and conduction, the columnar grains grew across pre-solidified layers. This situation led to fairly large grain formation in the vertical section: the examined maximum grain size in this section was found to be 390 μm (Fig. 4c). The horizontal section was found to have grains formed with a strong $\{101\}$ texture perpendicular to the build direction. The grain size was found to vary from 1.7 μm to 173 μm (Fig. 4c).

<Insert Figure 4>

Fig. 4d–f shows the crystallographic orientation and grain size distribution of the HIP-processed Hastelloy X sample. The typical LPBF columnar microstructure (Fig. 4a) could not be observed, and the EBSD obtained grain size were found to be smaller than the as-fabricated state in both the vertical and horizontal sections. The grains that formed were found to be less than 118 μm and 300 μm in the examined horizontal and vertical sections, respectively (Fig. 4f). Since the HIP treatment was conducted above Hastelloy X's recrystallisation temperature, significant changes in the microstructure occurred: the recrystallisation led to the formation of new grains and a fundamentally different kind of microstructure. The local deformation during the HIP processing, which generally functions as a driving force, was thought to be large enough to have promoted recrystallisation. This finding agreed with the observed microstructure shown in Fig. 3c–d, which shows that a large number of new grains had formed because of recrystallisation.

It should be noted that the true grain size after HIP treatment has increased, as seen in Fig. 3, noting that the scale is different in the before and after images. Because the fine columnar grains have grown epitaxially within the LPBF process, they have an orientation relationship and the EBSD sees them as much larger grains (Fig. 4a-b), so Fig. 4 is not showing the true grain size. During the HIP treatment, the

recrystallisation occurred and larger grains formed, but this texture relationship is disrupted and so the apparent grain size in EBSD decreased. This phenomenon has also been observed in the LPBF of Inconel 718 alloy [21,22], in which the grains were found to lose their strictly columnar morphology after HIP processing; microstructure homogeneity was instead promoted.

Fig. 5a shows a typical microcrack that was formed in the as-fabricated specimens. The microcrack was found to have formed along the HAGBs. Similar findings have also been reported in the literature [15,16]. The presence of Mo-rich carbides suggested that local enrichment of the solutes took place at the grain boundaries; the low melting liquid films lower the solid/liquid interface energy [23] and promote cracking by extensive wetting of the solid dendrites during the very last stage of solidification. Chauvet et al. [16] and other studies from the welding literature (e.g. [24]) have discussed the influences of thermal residual stress in triggering hot cracking. During successive layer-by-layer manufacturing, the top layer is under tensile stresses because its shrinkage is limited by the already solidified layers. These tensile stresses contribute to pulling on the liquid films, thus wetting the dendrites during the last stage of solidification.

<Insert Figure 5>

The most significant factor in determining the liquid feeding to compensate solidification shrinkage and deformation has not been established. The liquid fracture is generally assumed to be specifically related to an interdendritic pressure drop. Fig. 5b shows a schematic of a hot-tearing model, which illustrates the interdendritic liquid pressure drop at the dendrite root due to the insufficient liquid feeding to compensate solidification shrinkage and deformation. Generally, higher-pressure drops are associated with higher hot cracking susceptibility. The interdendritic liquid is assumed to fracture due to cavitation when the liquid pressure falls below a certain critical value [25,26]. The proposed hot-tearing model indicates that when the temperature reaches the coalescence temperature, bridging occurs between the dendrite's secondary arms, thus hindering the liquid feeding and finally giving rise to

the formation of hot cracks. One strategy in controlling the liquid pressure drop might be to control the Marangoni convection. Due to the rapid solidification and relatively small molten pool found within the LPBF process, however, it is fairly difficult to control the Marangoni convection and change the liquid pressure drop by optimising the LPBF process parameters.

3.3. Mechanical properties

3.3.1. Tensile performance

Fig. 6 and Table 2 show the tensile-testing results of the as-fabricated and HIP-processed specimens. The tensile performances of the three as-fabricated tensile specimens were found to be very consistent, with a 480 ± 10 MPa yield strength, 620 ± 15 MPa ultimate tensile strength, 149 ± 9 GPa Young's modulus and 40% elongation. Necking was observed at the fracture surface following the tensile test. The fairly high elongation (40%) observed implies that the samples showed ductile rather than brittle fracturing during testing. Compared to the as-fabricated tensile specimens, the HIP-processed specimens offered roughly 130 MPa and 60 MPa lower yield strength and ultimate tensile strength, respectively. These values could be attributed to the HIP processing in which recrystallisation took place. The true grain size has increased during HIP, so the yield strength and ultimate tensile strength decreased as expected. The change is relatively small, possibly because the texture of the sub-grains is not such an effective barrier to dislocation movement as they appear. The elongation, however, was not found to have exhibited a notable increase compared to the as-fabricated specimens. This finding differed from the literature [17], in which HIP processing has been found to contribute to around 10% improvement in elongation from 30% to 40% for an additive-manufactured Hastelloy X. This finding could be explained by the slight difference of the process parameters employed in both LPBF and HIP processing. Another possible factor that led to the similar elongation value within the two sets of samples in the present study could have been the gas-filled pores, which could have emerged from the original feedstock or may have formed within the LPBF process. These pores could not be closed by HIP processing.

<Insert Figure 6>

<Insert Table 2>

Fig. 7 shows the fracture surfaces of both the as-fabricated (Fig. 7a–d) and HIP-processed (Fig. 7e–h) Hastelloy X samples following the tensile test. The relatively high elongation (40%) was found to be associated with the necking behaviour in both samples; the microcracks that formed were further opened under the uniaxial loading in the as-fabricated sample (Fig. 7a). The cleavage-like surface observed in the as-fabricated specimens (Fig. 7b) indicates that the columnar grains were elongated along the length direction, which is parallel to the loading direction. This behaviour gave rise to the necking phenomenon as well as fracturing at the very last stage. It should also be noted that dendritic features were observed on the as-fabricated fracture surfaces (Fig. 7c), whereas they were not visible on the HIP-processed fracture surfaces (Fig. 7g). This situation occurred because the recrystallisation took place within the HIP processing, and the dendrites were not present in the HIP-processed specimens. The very fine dimple-like structure (dimple size of $<1\ \mu\text{m}$) implies local ductile behaviour for both the as-fabricated (Fig. 7d) and HIP-processed samples (Fig. 7h).

<Insert Figure 7>

3.3.2. Fatigue performance

Fig. 8 shows the as-fabricated and HIP-processed fatigue specimens used for stress-controlled fatigue testing. The dimensions of the specimens determined by ASTM standards are shown in Fig. 7a. The polished specimens exhibited fairly smooth surface finish, with a R_a roughness value of $0.33\ \mu\text{m}$ for fatigue testing (Fig.

8b–c). The S-N (stress/number of cycles) curves are plotted in Fig. 9 to show the fatigue performance of the as-fabricated and HIP-processed Hastelloy X specimens.

<Insert Figure 8>

The five-level maximum stresses (250–450 MPa) applied were determined based on the yield strength obtained from the tensile tests (Fig. 6 and Table 2). Overall, the fatigue life cycles for both as-fabricated and HIP-processed Hastelloy X specimens were found to increase with a decrease in the applied stress. For the as-fabricated specimens, the magnitude of the fatigue life cycles under 450 MPa was found to be 1×10^5 , which increased to 1×10^6 when the applied load was decreased to 250 MPa. The 1×10^5 fatigue life cycles that were obtained implies that the as-fabricated Hastelloy X specimens offered high-cycle fatigue performance (i.e. fatigue life $>10^4$ – 10^5 cycles), even though the applied stress approached the yield strength. Compared to the as-fabricated specimens, however, the HIP-processed Hastelloy X samples exhibited remarkable improvements in fatigue life. The effects of HIP processing were found to be more influential when the applied stress decreased during fatigue testing.

Under the stress of 450 MPa, the as-fabricated and HIP-processed specimens exhibited similar fatigue life levels, with an average fatigue life of 1.3×10^5 and 1.6×10^5 cycles, respectively. This situation indicated that the HIP processing had a very limited effect on the fatigue performance under this stress level, which occurs because the yield strength (350 MPa) of the HIP-processed samples is significantly lower compared to the applied stress of 450 MPa. The samples were subject to plastic deformation under every stress cycle, such that the cracks propagated fairly quickly once the cracks initiated, which accelerated the failure of the HIP-processed specimens.

<Insert Figure 9>

The obtained S-N curves indicated that the fatigue life cycles tended to be more scattered with reductions in the applied stress for both as-fabricated and HIP-processed specimens. This trend was more apparent in the HIP-processed specimens. Two factors may explain this situation. First, the material was approaching the endurance limit (and thus an asymptote in the S-N curve), which naturally provides some 'spread' in the material's lifetime under constant applied stress. Second, the surface defects and microcracks formed during the LPBF process are more influential in the lower stress associated with the higher-cycle regions, thus leading to more scattering in that region compared to the higher-stress regions [27]. The surface defects were taken into account, because it is impossible to eliminate all surface defects (e.g. microcracks and pores) by the polishing process and by HIP processing. One should also note that, when the applied stress was reduced to 250 MPa, the three HIP-processed specimens did not fail, even though they were subjected to 1×10^7 cycles. Thus, we may conclude that when the stress value is below 250 MPa, regardless of the number of cycles used, failure of the HIP-processed Hastelloy X will not occur. The failure criterion considered in fatigue testing is the rupture of the tested fatigue samples.

<Insert Figure 10>

Fig. 10 shows secondary electron SEM micrographs of the fatigue fracture surfaces under 300 MPa stress, which were useful for further fatigue-failure analysis. Fig. 10a1–4 shows the fracture surfaces of the as-fabricated Hastelloy X specimen, while Fig. 10b1–4 shows the fracture surfaces of the HIP-processed specimen. The fatigue life for the two specimens was measured to be 5.8×10^5 and 2.8×10^6 cycles, respectively. The improvement in fatigue life for the HIP-processed specimen shows agreement with the obtained fatigue-fracture surfaces (Fig. 10a1 and b1), in which the fracture region is smaller than that of the as-fabricated specimen.

Generally, fatigue failure proceeds via crack initiation, crack propagation and final failure at the site with the highest stress concentration, such as notches, pores or other types of local irregularities. Indeed, notches were found in both the as-fabricated and HIP-processed specimens, but the as-fabricated specimens seemed to exhibit multiple crack-initiation behaviours at the specimen's external surface. This situation may be explained by the cavities that form within the LPBF process, and cavities are generally associated with stress concentration. An apparent crack-initiation site was observed at the external surface shown in Fig. 10b2, which confirms that HIP processing could not close the surface's porosity. Furthermore, even if all the pores within the samples could be reduced in size by the HIP process, remaining defects (such as micropores) still had a strong impact on fatigue behaviour.

The crack growth region offered a distinct transition from stable to unstable crack growth for the as-fabricated specimen (Fig. 10a3), while no apparent transition was found for the HIP-processed specimen (Fig. 10b3). The HIP-processed Hastelloy X offered a larger and smoother crack-growth region than that of the as-fabricated specimen. This situation may be attributed to the microstructure and residual stress [28]. First, the columnar dendritic grain structure was predominant in the as-fabricated specimen, which gave rise to its anisotropy, while recrystallisation occurred in the HIP-processed Hastelloy X, which instead promoted the microstructure's homogeneity. Second, thermal gradient-induced residual stress remained in the LPBF as-fabricated specimens, and the residual stress together with the cyclic stress promoted the propagation of cracks once the cracks were initiated. The HIP processing, however, released the residual stress in the HIP-processed specimens, such that the fatigue durability was enhanced. Striations were observed in the stable crack growth region in both the as-fabricated and HIP-processed Hastelloy X samples, while secondary cracks were only observed in the as-fabricated specimen (Fig. 10a4–b4). Fig. 10a4 also indicates the elongation and fracture behaviour of the columnar grains under cyclic stress. This behaviour gave rise to a rough crack growth surface in the as-fabricated Hastelloy X.

<Insert Figure 11>

Fig. 11 shows the fatigue-fracture surfaces of as-fabricated and HIP-processed specimens under the stress of 450 MPa. The fracture region area for both the as-fabricated and HIP-processed samples exhibited similar size but were much larger than the 300 MPa specimens (Fig. 10). Compared to the as-fabricated specimen, the HIP-processed specimen displayed a similar fatigue life cycle under the stress of 450 MPa, even though most of the internal pores and cracks were closed, and residual stress release had been achieved. This situation could be attributed to the relatively high cyclic stress (450 MPa) that was applied, which was beyond the yield strength of 350 MPa, such that under each stress cycle, the specimen was subject to plastic deformation.

The crack-initiation site where stress concentration occurred was assumed to have been stimulated by the plastic deformation, and the crack propagated fairly quickly once the crack was initiated. Several unmelted Hastelloy X particles were observed in the crack-initiation sites, where pores were formed within the LPBF process, and they were very close to the samples' external surfaces (Fig. 11a2 and b2). This situation implies that the LPBF process formed pores that were filled with inert gas, which cannot be closed by HIP processing. A very fine dimple microstructure (dimple size $<1 \mu\text{m}$) was observed in the two samples' fracture regions (Fig. 11 a3 and b3). This type of dimple microstructure was found to be very similar to the tensile fracture structure (Fig. 7).

4. Discussion

This study's experimental results have demonstrated that microcracking is the primary defect within the LPBF of Hastelloy X. The microcracks could not be eliminated even under the optimal conditions; the relative density achieved was 99.3%. The HIP processing was found to close all the microcracks and most of the internal pores by applying high temperature and high pressure. This heat treatment also caused recrystallisation during the fairly long holding time of 3 hours. This situation contributed to a ~ 130 MPa decrease in yield strength compared to the as-fabricated Hastelloy X specimens. The 99.98% relative density of the HIP-processed samples suggests that a very small number of residual pores remained in the HIP-

processed Hastelloy X that could not be eliminated by HIP processing. Fig. 2g shows the residual pores that were observed within the HIP-processed sample, with an average size of 5.6 μm (measured by ImageJ). This finding shows agreement with the literature [22], in which the additive-manufactured Inconel 718 was post-processed by HIP processing. The authors have found that the relative density can be improved to 99.985%–99.989% by employing HIP. This effect could be explained by the entrapped argon during the LPBF process: the argon filled in the cavities and counteracted the pressure applied during HIP processing. Thus, all the microcracks that formed within the LPBF process may be concluded to have been gas-free cracks that could be closed by HIP processing, while the very small number of gas-filled pores could not be closed. The percentage of the residual pores was measured to be 0.02% in the present study.

In addition to tensile strength, HIP processing was also found to significantly affect fatigue behaviour. The HIP processing contributed to fatigue performance, and the influence of the processing was found to be more influential in the high-cycle fatigue regime. This finding could be explained by two factors. First, during the crack-initiation stage, stress concentration was the dominant factor to promote crack initiation. Due to the closing of microcracks and cavities by HIP processing, the stress concentration around the micropores inside the Hastelloy X was reduced. Second, during the crack-propagation stage, residual stress played a significant role in determining the fatigue behaviour. In addition to the closing of microcracks and pores, HIP processing also enabled residual stress release. Thus, the plastic deformation of the specimens was decreased, while the fatigue performance was improved. In the present study, the as-fabricated and HIP-processed specimens exhibited similar fatigue life values under the applied maximum stress of 450 MPa. This occurred because the applied stress was higher than the yield strength of 350 MPa of the HIP-processed samples, so plastic deformation occurred under every cyclic loading condition.

5. Conclusions

This study has investigated the effects of hot isostatic processing (HIP) on laser powder bed fusion (LPBF) of Hastelloy X. The fatigue performance in particular was systematically examined for the first time in this work. This study has also highlighted

the hot cracking mechanism and has presented the following important findings derived from the experimental results.

- (1) An optimal 200 mm/s scanning speed and 90 μm hatch spacing were determined by quantifying the relative density of the as-fabricated cubic samples ($10 \times 10 \times 10 \text{ mm}^3$) using the Archimedes method. The relative density was found to be as high as 99.3% under the optimal process parameters, with a small number of pores and microcracks also observed.
- (2) Hot isostatic pressing was found to be capable of closing all internal microcracks and gas-free micropores by applying high temperature and high pressure. The small number of residual pores observed showed agreement with the 99.98% relative density obtained in the HIP-processed samples. Microcracks were not observed in the HIP-processed samples, which implies that all the microcracks that formed were gas-free and thus could be closed by HIP processing. The residual pores, however, were gas-filled and could not be eliminated by HIP processing, which implies that HIP processing cannot contribute to a 100% density value.
- (3) Compared to the as-fabricated specimens, the HIP-processed Hastelloy X was roughly 130 MPa and 60 MPa weaker in yield strength and ultimate tensile strength, respectively, which was attributed to microstructure changes and recrystallisation. The HIP-processed specimens exhibited significant improvement in fatigue life: the effects of HIP processing were found to be more influential when the applied stress decreased during fatigue testing (high cycle regime), because the HIP processing managed to reduce the stress concentration sites by closing internal porosity and achieving residual stress release so that the fatigue endurance limit was enhanced.
- (4) In terms of the inspected both vertical and horizontal sections by SEM and OM, the microcracks distribution is not found to be location dependent, they are distributed fairly uniformly instead. However, they are found to be formed along the high angle grain boundaries (HAGBs) rather than the low angle grain boundaries (LAGBs) through the EBSD. In addition to conditions proposed in the literature, the interdendritic liquid pressure drop was found to be another significant factor in intergranular microcrack formation.

These results indicate that microcracking is the primary defect in the LPBD of Hastelloy X, while HIP is capable of closing most of the internal cracks and pores. The disadvantages of HIP processing, however, include extra post-processing cost and a certain degree of sacrifice of tensile strength. In terms of the hot cracking mechanism, since the hot cracking tends to occur along the HAGBs, further study of LPBF process parameter optimisation might be necessary in order to reduce the HAGB fraction in as-fabricated Hastelloy X parts. In addition, since the pressure drop between the dendrite tip and root contributes to hot cracking during columnar grain growth, further study of the thermodynamic properties of molten pools should be conducted in order to have a better understanding of hot cracking formation.

Acknowledgements

The authors would like to thank Dr. Sasan Dadbakhsh from KU Leuven, Belgium for the valuable discussions and tensile-testing operations. The lead author greatly appreciates the financial support of Cardiff University–KU Leuven strategic scholarship and ASTUTE 2020.

References

- [1] H.U. Hong, I.S. Kim, B.G. Choi, H.W. Jeong, C.Y. Jo, Effects of temperature and strain range on fatigue cracking behavior in Hastelloy X, *Mater. Lett.* 62 (2008) 4351–4353. doi:10.1016/j.matlet.2008.07.032.
- [2] J.C. Zhao, M. Larsen, V. Ravikumar, Phase precipitation and time-temperature-transformation diagram of Hastelloy X, *Mater. Sci. Eng. A.* 293 (2000) 112–119. doi:10.1016/S0921-5093(00)01049-2.
- [3] N.J. Harrison, I. Todd, K. Mumtaz, Reduction of micro-cracking in nickel superalloys processed by Selective Laser Melting: A fundamental alloy design approach, *Acta Mater.* 94 (2015) 59–68. doi:10.1016/j.actamat.2015.04.035.
- [4] M.M. Attallah, R. Jennings, X. Wang, L.N. Carter, Additive manufacturing of Ni-based superalloys: The outstanding issues, *MRS Bull.* 41 (2016) 758–764. doi:10.1557/mrs.2016.211.
- [5] Q. Han, R. Setchi, S.L. Evans, Synthesis and characterisation of advanced ball-milled Al-Al₂O₃ nanocomposites for selective laser melting, *Powder Technol.* 297 (2016) 183–192. doi:10.1016/j.powtec.2016.04.015.
- [6] Q. Han, Y. Geng, R. Setchi, F. Lacan, D. Gu, S.L. Evans, Macro and nanoscale wear behaviour of Al-Al₂O₃ nanocomposites fabricated by selective laser melting, *Compos. Part B Eng.* 127 (2017) 26–35. doi:10.1016/j.compositesb.2017.06.026.
- [7] H. Rao, S. Giet, K. Yang, X. Wu, C.H.J. Davies, The influence of processing

- parameters on aluminium alloy A357 manufactured by Selective Laser Melting, *Mater. Des.* 109 (2016) 334–346. doi:10.1016/j.matdes.2016.07.009.
- [8] Q. Han, R. Setchi, F. Lacan, D. Gu, S.L. Evans, Selective laser melting of advanced Al-Al₂O₃ nanocomposites: Simulation, microstructure and mechanical properties, *Mater. Sci. Eng. A.* 698 (2017) 162–173. doi:10.1016/j.msea.2017.05.061.
- [9] P. Zhang, Z.J. Zhang, L.L. Li, Z.F. Zhang, Twin boundary: Stronger or weaker interface to resist fatigue cracking?, *Scr. Mater.* 66 (2012) 854–859. doi:10.1016/j.scriptamat.2012.01.028.
- [10] Z. Xu, C.J. Hyde, A. Thompson, R.K. Leach, I. Maskery, C. Tuck, A.T. Clare, Staged thermomechanical testing of nickel superalloys produced by selective laser melting, *Mater. Des.* 133 (2017) 520–527. doi:10.1016/j.matdes.2017.08.009.
- [11] L.N. Carter, X. Wang, N. Read, R. Khan, M. Aristizabal, K. Essa, M.M. Attallah, Process optimisation of selective laser melting using energy density model for nickel based superalloys, *Mater. Sci. Technol.* 0 (2015) 1743284715Y.000. doi:10.1179/1743284715Y.0000000108.
- [12] F. Wang, X.H. Wu, D. Clark, On direct laser deposited Hastelloy X: dimension, surface finish, microstructure and mechanical properties, *Mater. Sci. Technol.* 27 (2011) 344–356. doi:10.1179/026708309X12578491814591.
- [13] D. Tomus, T. Jarvis, X. Wu, J. Mei, P. Rometsch, E. Hery, J.F. Rideau, S. Vaillant, Controlling the microstructure of Hastelloy-X components manufactured by Selective Laser Melting, in: *Phys. Procedia*, 2013: pp. 823–827. doi:10.1016/j.phpro.2013.03.154.
- [14] D. Tomus, P.A. Rometsch, M. Heilmaier, X. Wu, Effect of minor alloying elements on crack-formation characteristics of Hastelloy-X manufactured by selective laser melting, *Addit. Manuf.* 16 (2017) 65–72. doi:10.1016/j.addma.2017.05.006.
- [15] G. Marchese, G. Basile, E. Bassini, A. Aversa, M. Lombardi, D. Ugues, P. Fino, S. Biamino, Study of the microstructure and cracking mechanisms of hastelloy X produced by laser powder bed fusion, *Materials (Basel)*. 11 (2018). doi:10.3390/ma11010106.
- [16] E. Chauvet, P. Kontis, E.A. Jäggle, B. Gault, D. Raabe, C. Tassin, J.J. Blandin, R. Dendievel, B. Vayre, S. Abed, G. Martin, Hot cracking mechanism affecting a non-weldable Ni-based superalloy produced by selective electron Beam Melting, *Acta Mater.* 142 (2018) 82–94. doi:10.1016/j.actamat.2017.09.047.
- [17] D. Tomus, Y. Tian, P.A. Rometsch, M. Heilmaier, X. Wu, Influence of post heat treatments on anisotropy of mechanical behaviour and microstructure of Hastelloy-X parts produced by selective laser melting, *Mater. Sci. Eng. A.* 667 (2016) 42–53. doi:10.1016/j.msea.2016.04.086.
- [18] T. Etter, K. Kunze, F. Geiger, H. Meidani, Reduction in mechanical anisotropy through high temperature heat treatment of Hastelloy X processed by Selective Laser Melting (SLM), *IOP Conf. Ser. Mater. Sci. Eng.* 82 (2015) 12097. doi:10.1088/1757-899X/82/1/012097.
- [19] Y. Tian, D. Tomus, P. Rometsch, X. Wu, Influences of processing parameters on surface roughness of Hastelloy X produced by selective laser melting, *Addit. Manuf.*

- 13 (2017) 103–112. doi:10.1016/j.addma.2016.10.010.
- [20] F. Wang, Mechanical property study on rapid additive layer manufacture Hastelloy?? X alloy by selective laser melting technology, *Int. J. Adv. Manuf. Technol.* 58 (2012) 545–551. doi:10.1007/s00170-011-3423-2.
- [21] L. Chang, W. Sun, Y. Cui, R. Yang, Influences of hot-isostatic-pressing temperature on microstructure, tensile properties and tensile fracture mode of Inconel 718 powder compact, *Mater. Sci. Eng. A.* 599 (2014) 186–195. doi:10.1016/j.msea.2014.01.095.
- [22] W. Tillmann, C. Schaak, J. Nellesen, M. Schaper, M.E. Aydinöz, K.P. Hoyer, Hot isostatic pressing of IN718 components manufactured by selective laser melting, *Addit. Manuf.* 13 (2017) 93–102. doi:10.1016/j.addma.2016.11.006.
- [23] J. DuPont N., J. Lippold C., S. Kiser D., *Welding Metallurgy and Weldability of Nickel Based Alloys*, 2009. doi:10.1017/CBO9781107415324.004.
- [24] J. Zhang, R.F. Singer, Hot tearing of nickel-based superalloys during directional solidification, *Acta Mater.* 50 (2002) 1869–1879. doi:10.1016/S1359-6454(02)00042-3.
- [25] M. Rappaz, J.-M. Drezet, M. Gremaud, A new hot-tearing criterion, *Metall. Mater. Trans. A.* 30 (1999) 449–455. doi:10.1007/s11661-999-0334-z.
- [26] N. Coniglio, C.E. Cross, Initiation and growth mechanisms for weld solidification cracking, *Int. Mater. Rev.* 58 (2013) 375–397. doi:10.1179/1743280413Y.0000000020.
- [27] B. Van Hooreweder, Y. Apers, K. Lietaert, J.P. Kruth, Improving the fatigue performance of porous metallic biomaterials produced by Selective Laser Melting, *Acta Biomater.* 47 (2017) 193–202. doi:10.1016/j.actbio.2016.10.005.
- [28] S. Leuders, M. Thöne, A. Riemer, T. Niendorf, T. Tröster, H.A. Richard, H.J. Maier, On the mechanical behaviour of titanium alloy TiAl6V4 manufactured by selective laser melting: Fatigue resistance and crack growth performance, *Int. J. Fatigue.* 48 (2013) 300–307. doi:10.1016/j.ijfatigue.2012.11.011.

Figures

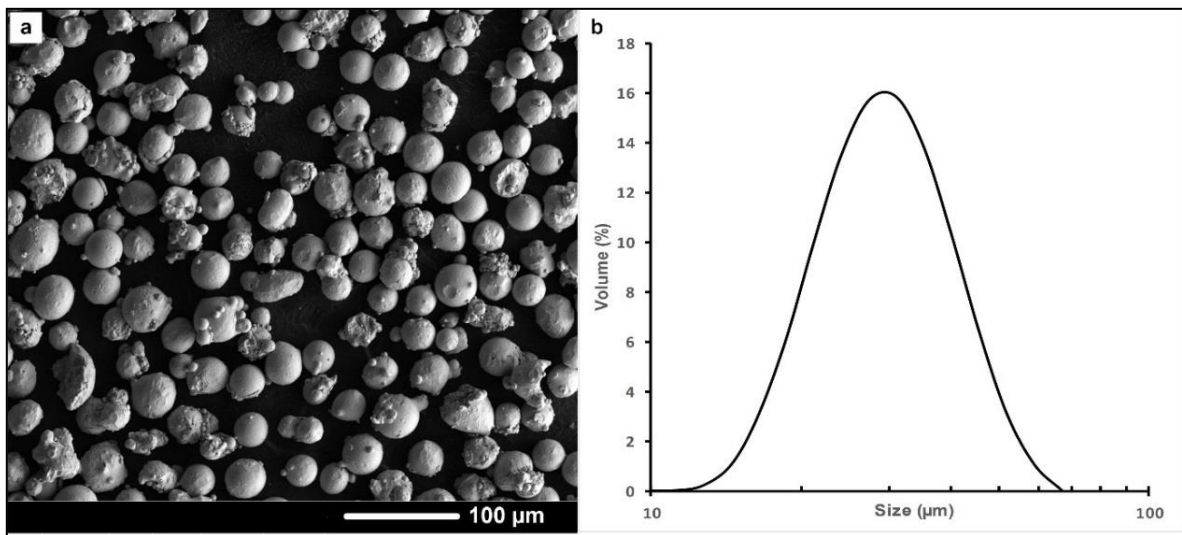


Fig. 1. Raw powder material: (a) morphology of raw Hastelloy X; (b) particle size distribution.

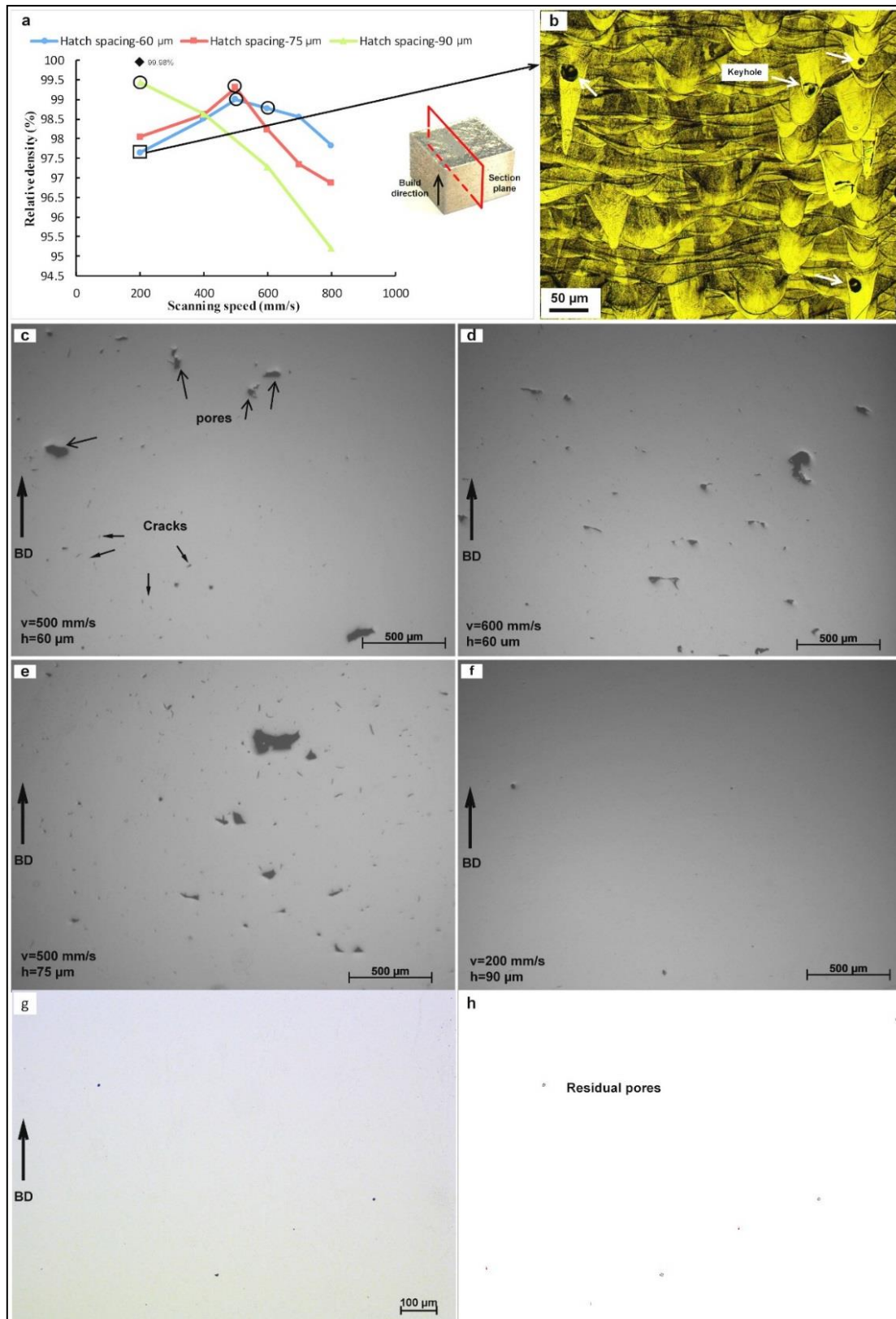


Fig. 2. Relative density of the as-fabricated and HIP-processed samples: (a) relative density measured by the Archimedes method; (b–f) OM micrographs showing the porosity and microcracks in the as-fabricated vertical sections under different conditions; (g) OM micrograph showing the porosity of the HIP-processed sample; (h) porosity distribution from (g) processed by ImageJ software; the arrow indicates the build direction.

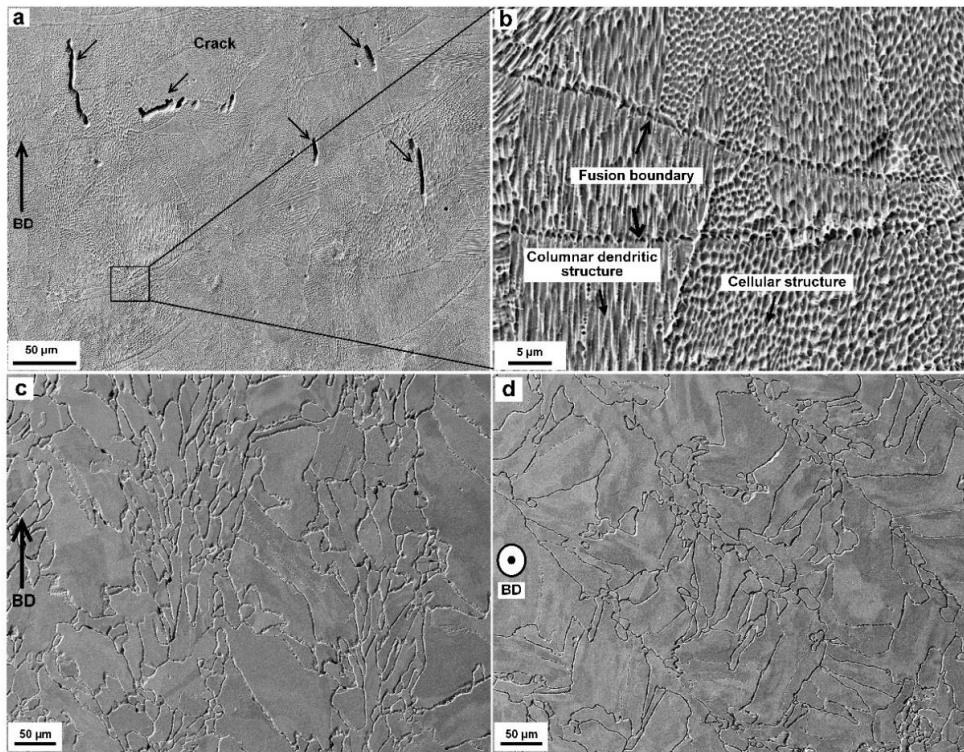


Fig. 3. Secondary electron SEM micrographs showing the microstructure of as-fabricated and HIP-processed Hastelloy X samples: (a–b) microstructure of the as-fabricated sample in vertical section; (c–d) microstructure of vertical and horizontal sections of the HIP-processed sample.

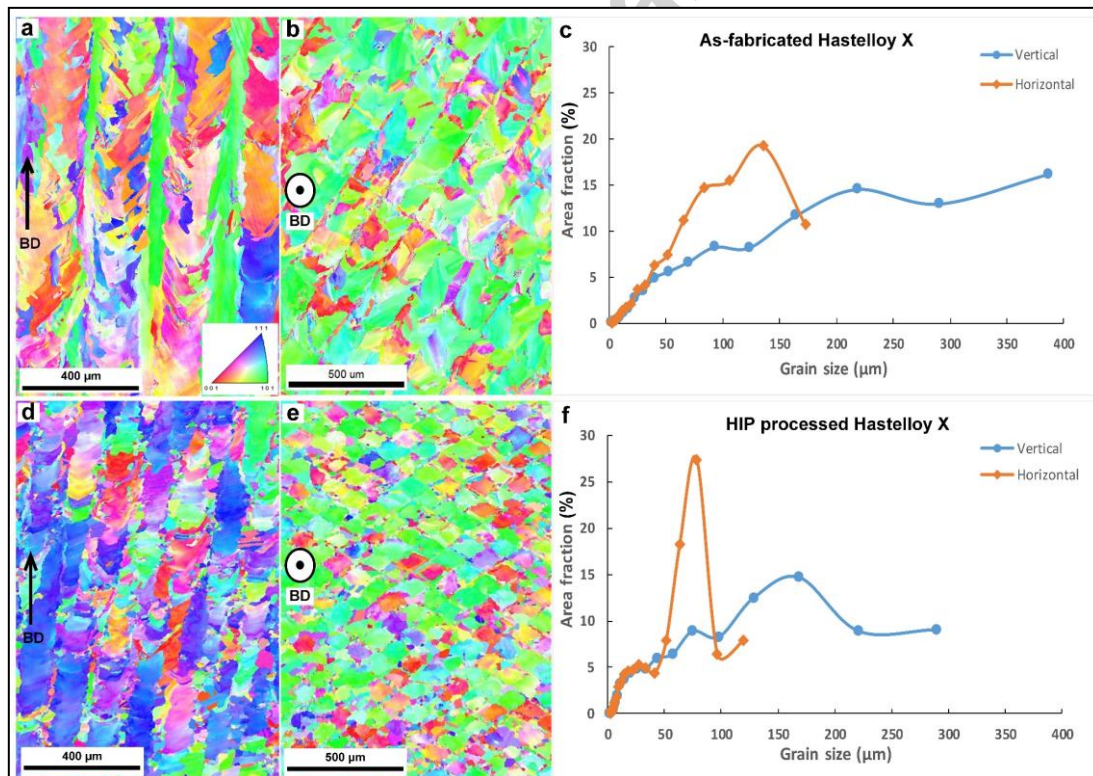


Fig. 4. EBSD crystallographic orientation maps and grain size distribution: (a–c) maps and grain size distribution of the vertical and horizontal sections in the as-fabricated sample; (d–f) orientation maps and grain size distribution in the HIP-processed Hastelloy X sample.

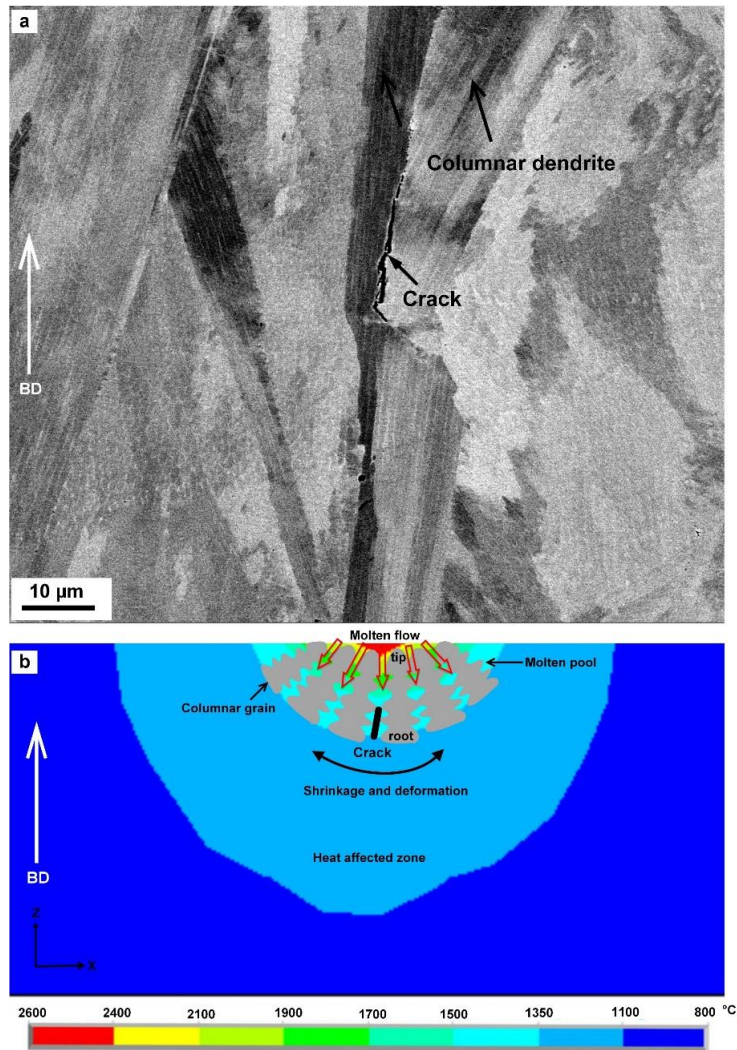


Fig. 5. Hot cracking mechanism: (a) backscattered electron SEM micrographs showing a typical microcrack; (b) schematic of the cracking mechanism.

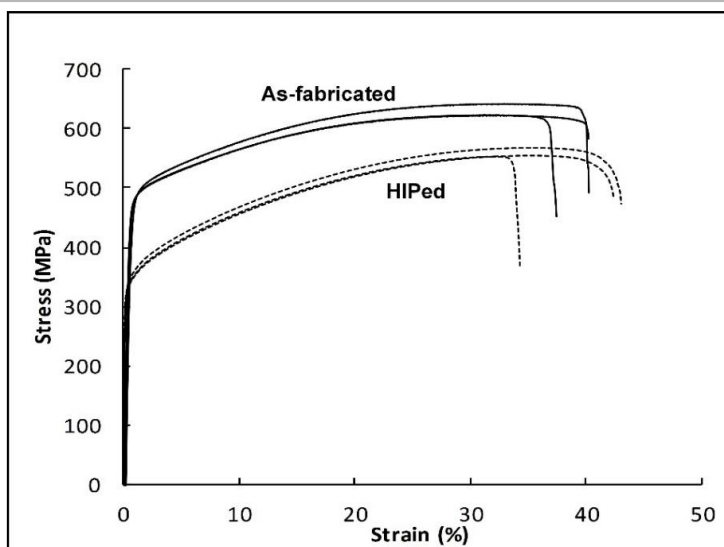


Fig. 6. Tensile stress-strain curves of as-fabricated and HIP-processed Hastelloy X samples.

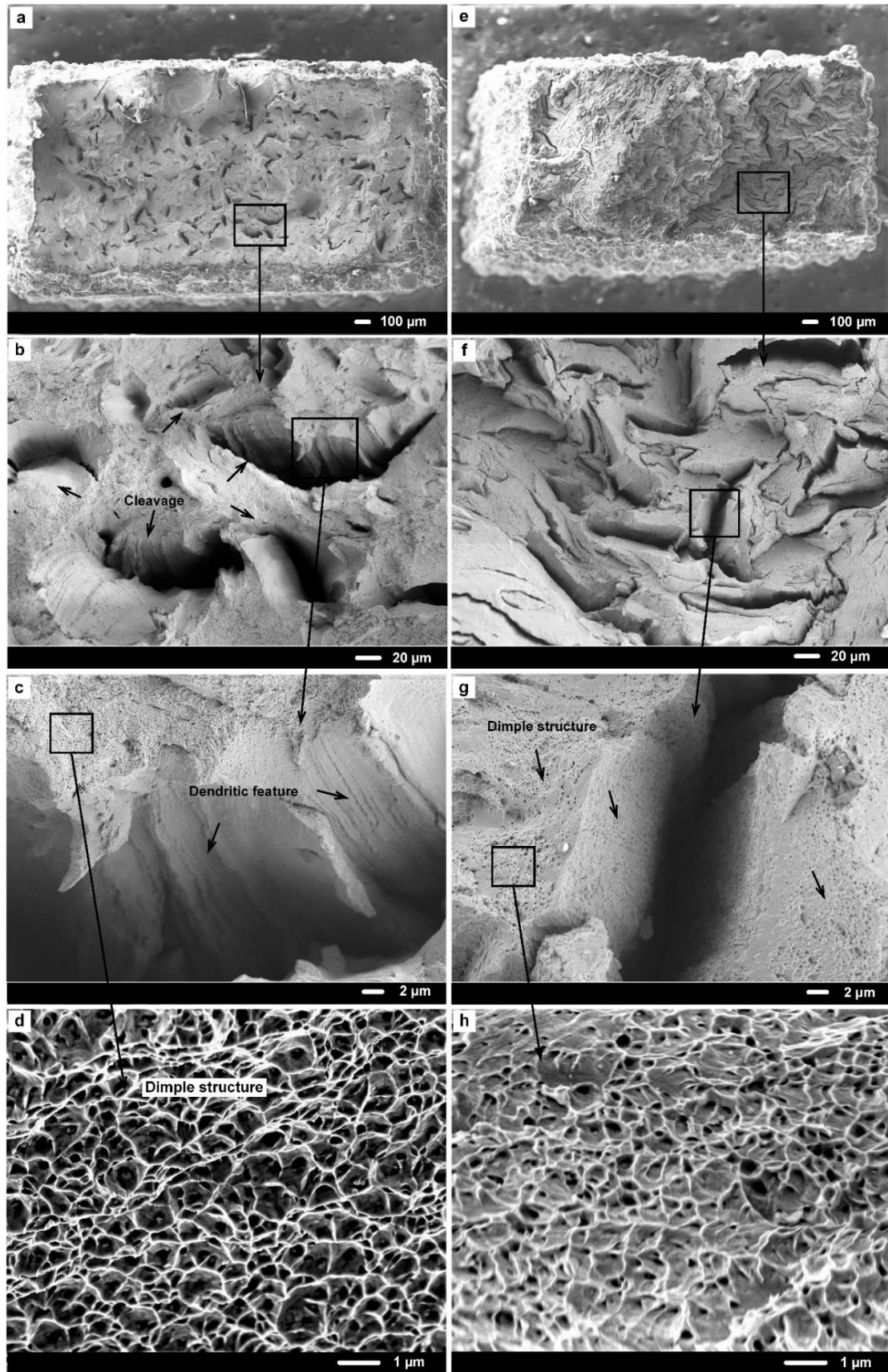


Fig. 7. Secondary electron SEM micrographs showing the fracture surfaces of: (a–d) as-fabricated Hastelloy X sample; (e–h) HIP-processed Hastelloy X sample.

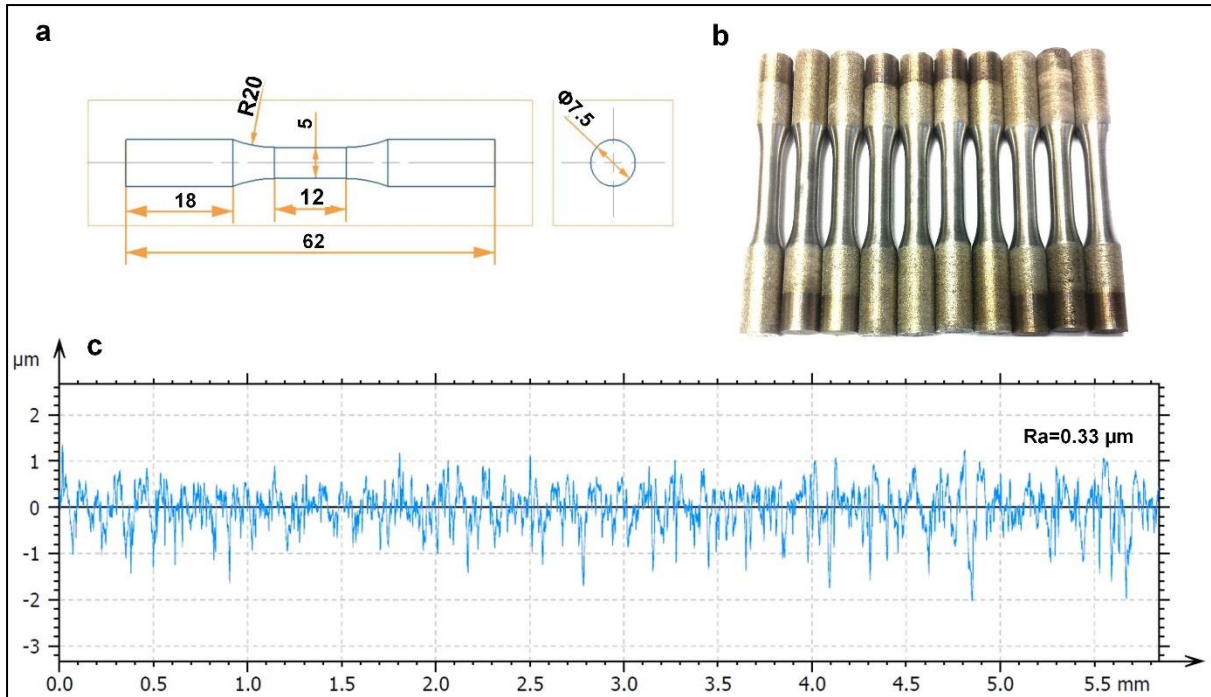


Fig. 8. The fabricated Hastelloy X fatigue samples: (a) dimensions of the fatigue specimens; (b) part of the polished fatigue specimens; (c) the polished surface, showing a R_a roughness value of $0.33 \mu\text{m}$.

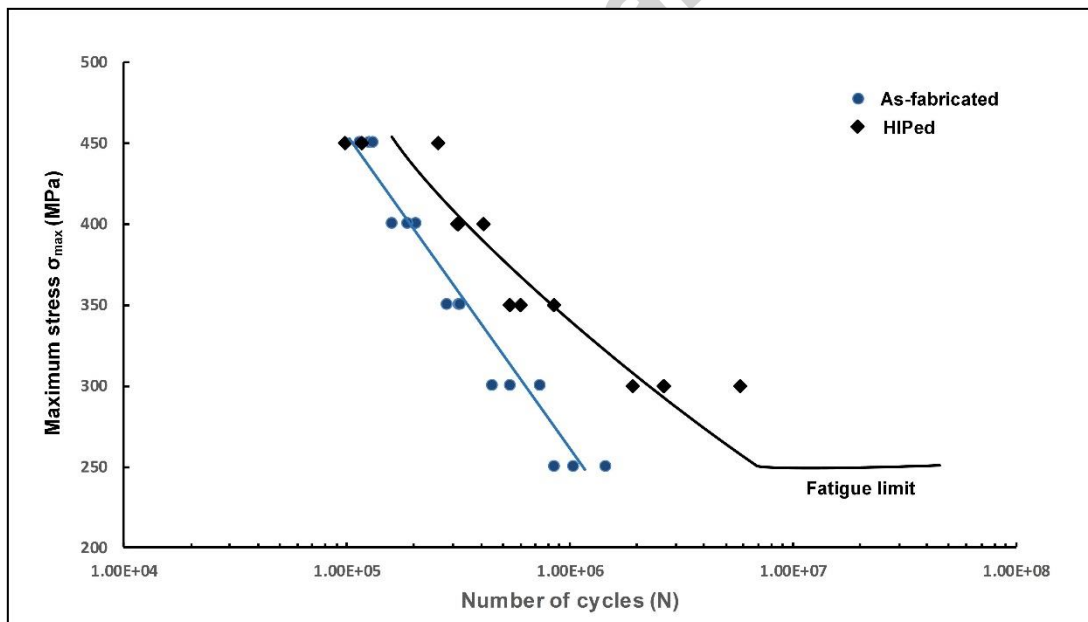


Fig. 9. Fatigue performance of the as-fabricated and HIP-processed Hastelloy X specimens.

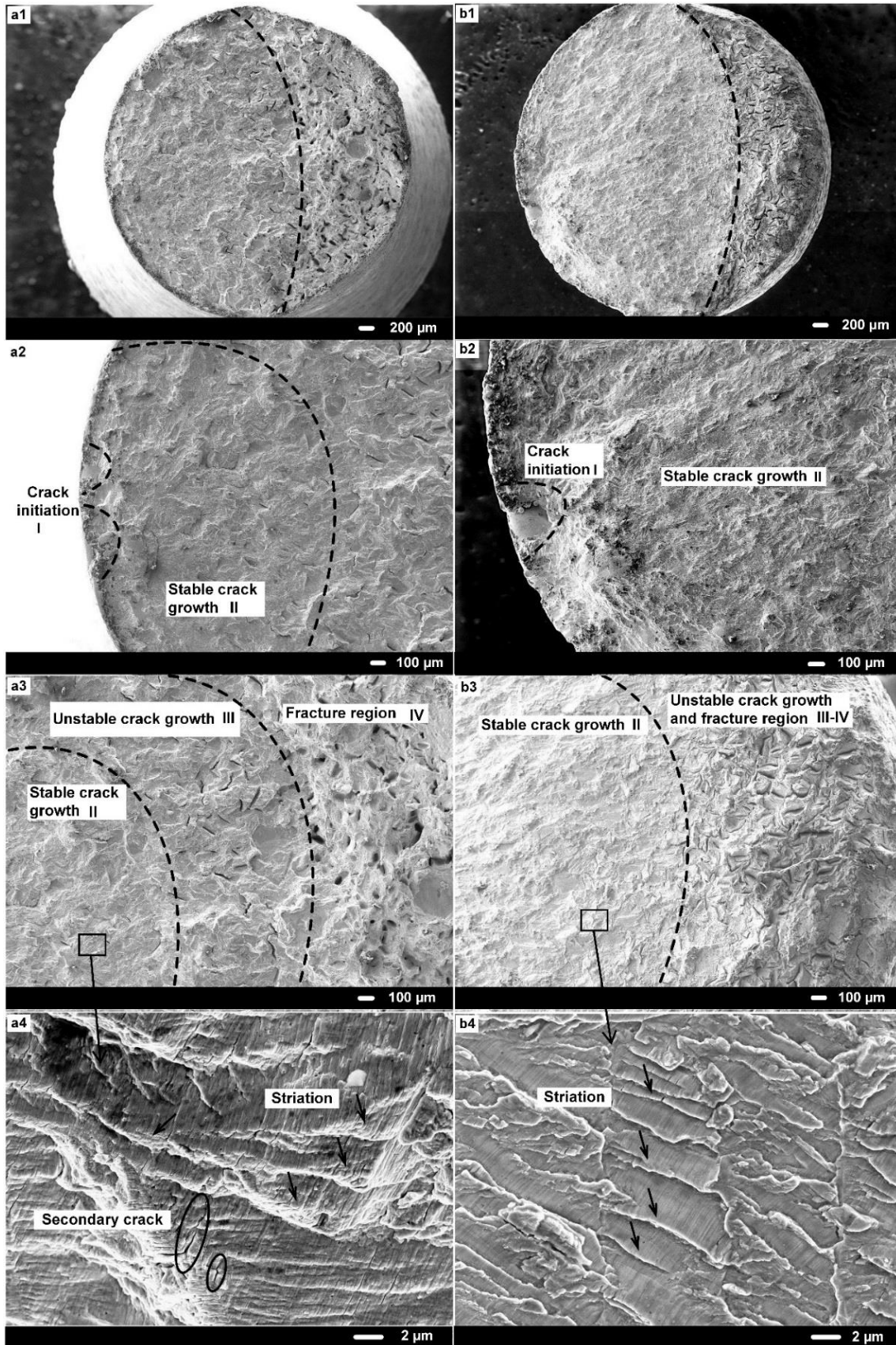


Fig. 10. Secondary electron SEM micrographs showing fatigue-fracture surfaces of as-fabricated (a1–4) and HIP-processed specimens (b1–4) under 300 MPa stress.

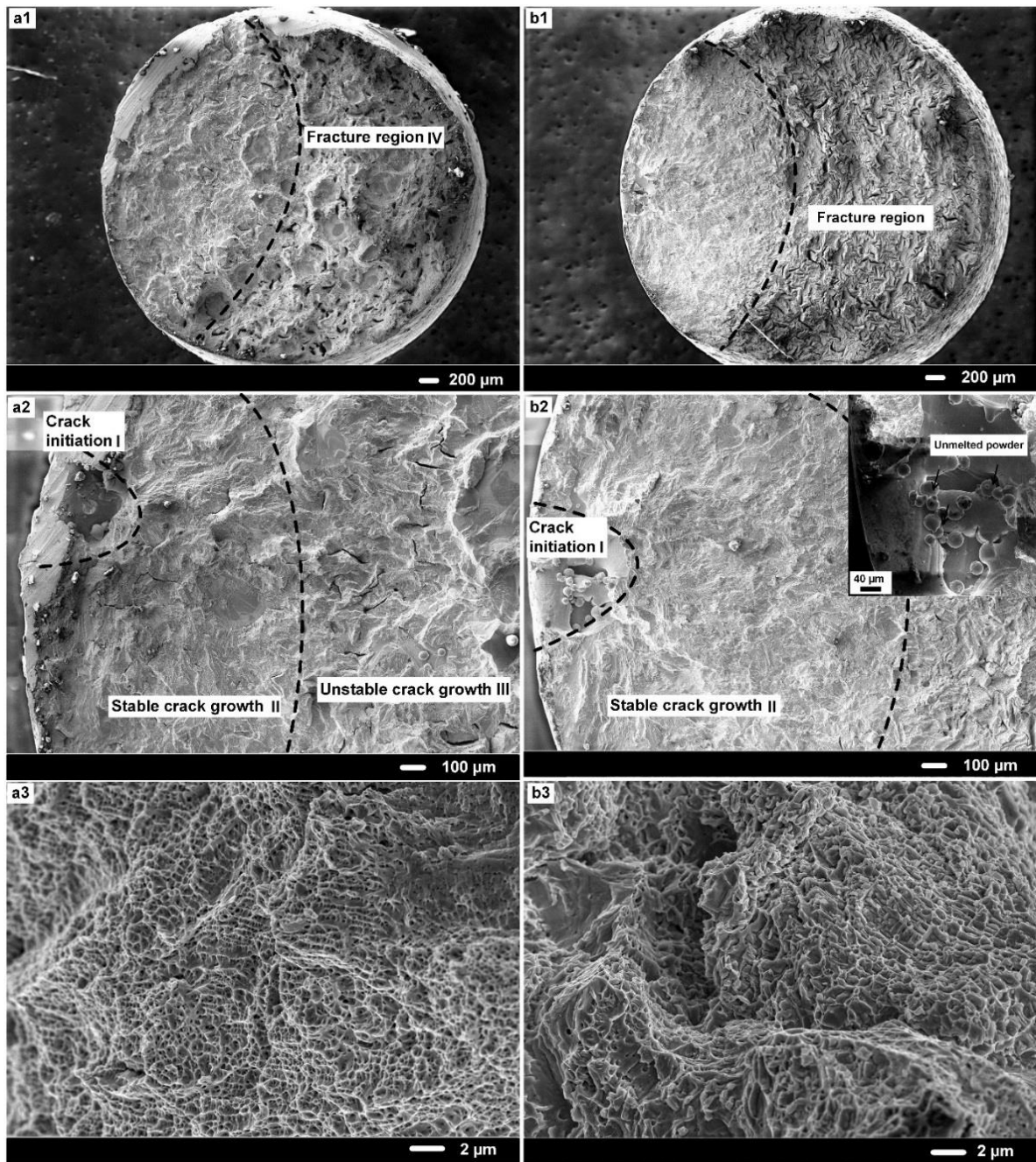


Fig. 11. Secondary electron SEM micrographs showing fatigue-fracture surfaces of as-fabricated (a1–3) and HIP-processed specimens (b1–3) under the stress of 450 MPa.

Tables

Table 1.

Process parameters.

Parameter	Value	Parameter	Value
Laser power (W)	95	Scanning speed (mm/s)	200–800
Beam diameter (μm)	50	Hatch spacing (μm)	60, 75, 90
Layer thickness (μm)	30	Scanning strategy	Bidirectional scanning with 90° rotation between layers

Table 2.

Mechanical properties from tensile tests of as-fabricated and HIP samples.

Category	Young's modulus (GPa)	Yield strength (MPa)	Ultimate tensile strength (MPa)	Elongation (%)
As-fabricated	149 \pm 9	480 \pm 10	620 \pm 15	40 \pm 1
HIP-processed	150 \pm 5	350 \pm 6	560 \pm 9	41 \pm 4